Frontiers in Health Informatics
ISSN-Online: 2676-7104
www.healthinformaticsjournal.com
2024; Vol 13: Issue 8
Open Access

Design and Formulation of Dual-Action Nanoparticles for Synergistic Cancer Therapy

Santanu Mallik[1], Nakul Gupta[2], Pushkar Kumar Ray[3], Suraj Mandal[4], Akshay Mangavade[5], Jatin Sharma[6], Bharatbhusan Sahu[7], T. Naga Aparna[8*]

[1]Associate Professor, Bharat Pharmaceutical Technology, Amtali, Agartala, West Tripura-799130
[2]Director and Professor, IIMT College of Pharmacy, Knowledge Park-III, Greater Noida, Uttar Pradesh 201310, India
[3]IIMT College of Pharmacy, Plot No. 19 & 20, Knowledge Park III, Greater Noida, Uttar Pradesh 201310, India
[4]Department of Pharmacy, IIMT College of Medical Sciences, IIMT University, O-Pocket, Ganganagar, Meerut, 250001, Uttar Pradesh, India
[5]Assistant Professor, University of Mumbai
[6]Postdoctoral (LLD), Sardar Patel Subharti Institute of Law, Subharti University
[7]Assistant Professor, Centurion University of Technology and Management, Odisha, India, 765002
[8]Associate Professor, G. Pulla Reddy College of Pharmacy, Mehdipatnam, Hyderabad 500028
Corresponding Email: T. Naga Aparna, nagaaparna4@gmail.com

Cite this paper as: Santanu Mallik, Nakul Gupta, Pushkar Kumar Ray, Suraj Mandal, Akshay Mangavade, Jatin Sharma, Bharatbhusan Sahu, T. Naga Aparna (2024) Design and Formulation of Dual-Action Nanoparticles for Synergistic Cancer Therapy, *Frontiers in Health Informatics*, *13* (8), 2117-2134

Abstract
Suboptimal tumour targeting, systemic toxicity, and drug resistance are three of the major obstacles in cancer treatment. To improve accuracy of tumour targeting, effectiveness, and safety, dual-action nanoparticles combine two or more therapeutic processes onto one platform. Designing and formulating CS-g-PNIPAAm nanoparticles loaded with oxaliplatin is the main focus of this investigation. The nanoparticles release their medications preferentially in tumor-specific acidic and high-temperature settings, demonstrating thermo- and pH-responsiveness. High drug-loading efficiency (82.8%) and great stability with low damage to normal cells were obtained by the nanoparticles by direct loading and self-assembly procedures. Research in vitro has shown that compared to free medicines, they had better cytotoxicity against cancer cells, improved cellular absorption, and effective drug release under tumor-relevant circumstances. These results highlight the promise of dual-action nanoparticles for improving targeted cancer therapy and escaping the constraints of traditional therapies.
Keywords: Dual-action nanoparticles, cancer therapy, oxaliplatin, thermo-responsive, pH-sensitive, drug delivery

1. Introduction

As one of the top causes of death and disability on a global scale, cancer is an ongoing threat to public health across the globe. Systemic toxicity, drug resistance, and poor tumour targeting are still constraints of current treatment methods, even if they have advanced significantly (He et al., 2016; Da Silva et al., 2016). Novel strategies for cancer therapy are required in light of these obstacles. Among new approaches, dual-action nanoparticles stand up as a promising tactic that might revolutionise cancer treatment. These technologies allow for targeted tumour targeting, less off-target toxicity, and improved treatment effectiveness by combining many therapeutic pathways into a single nanoplatform.

New developments in nanotechnology have opened the door to the possibility of creating multifunctional nanoparticles that can carry imaging agents, biomolecules, and chemotherapeutics all at once. Taking use of acidic pH, overexpressed enzymes, and increased permeability and retention (EPR) effects, these platforms aim to circumvent the constraints of traditional therapeutics (Zhang et al., 2020; Liu et al., 2019). One example is

the use of enzyme-responsive nanoparticles, which may selectively activate therapeutic medicines in tumours while causing little harm to healthy tissues (Chen et al., 2018). Similarly, pH-sensitive devices maximise therapeutic efficacy by achieving site-specific drug release in the acidic tumour environment (Baby et al., 2021). Particularly encouraging is the idea of synergistic treatment using nanoparticles with dual-action properties. A chemotherapeutic drug that causes DNA damage and an immunomodulator that boosts anti-tumor immune responses are two examples of medicines with complementary action mechanisms that may be administered together to produce synergy (Shim et al., 2017; Wu et al., 2020). By attacking the tumour from many angles at once, this method improves the therapeutic result and decreases the chance of resistance. The effectiveness of co-delivering oxaliplatin and proteins utilising a nanoparticle technology was established by He et al. (2016), demonstrating the possibility of such combinations in clinical settings.

Their ability to respond to stimuli is another attractive feature of dual-action nanoparticles. Systems that are designed to respond to certain stimuli, such light, temperature, or enzymes, are known as stimuli-responsive systems (Ashrafizadeh et al., 2021; Cao et al., 2019). For instance, thermoresponsive nanoparticles may allow for regulated medication release at the tumour site by exhibiting a phase shift at a predetermined temperature. Enhancing medication bioavailability and reducing systemic exposure are two areas where these characteristics really shine. By creating thermoresponsive nanoparticles that were able to provide precision photothermal treatment, Liu et al. (2019) demonstrated the possibility of combining many functions into one system.

Customisation is another strength of nanoparticle-based systems that allows them to be used in a variety of ways. There has been much research on the potential of polymer-based dendrimers, liposomes, and nanoparticles to transport diagnostic and therapeutic substances (Zhang et al., 2017; Birrenbach & Speiser, 1976). Polymer nanoparticles with pH-triggered release and adjustable drug loading were described by Baby et al. (2021), laying the groundwork for tailoring medication delivery to individual patients. Similarly, Wu et al. (2020) found that treatment effectiveness was significantly improved when docetaxel and cisplatin were co-delivered using lipid-polymer hybrid nanoparticles.

There is still a long way to go before dual-action nanoparticles may be used in clinical practice, despite their promising future. Problems with stability, regulatory approval, and large-scale synthesis must be resolved. Nevertheless, these obstacles are being gradually overcome by advancements in nanotechnology and pharmaceutical sciences, which are bringing these sophisticated systems closer to clinical use (Couvreur, 2013; Wang et al., 2021). As shown by the approval of liposomal formulations for cancer treatment (Krauss et al., 2019), regulatory frameworks are also changing to accommodate the difficulties of formulations based on nanoparticles.

The purpose of this article is to go into the topics of cancer synergistic treatment using dual-action nanoparticles, including their design, formulation, and use. We provide a thorough review of these systems' potential to transform cancer therapy by combining findings from new research and using modern approaches. This work examines the design, physicochemical characteristics, and therapeutic efficiency of oxaliplatin-loaded nanoparticles using them as a model system. Results add to mounting evidence that dual-action nanoparticles may help cancer patients overcome treatment's many obstacles.

2. Materials and Methods

2.1 Chemicals Used

The following materials, either AR/LR grade or the best available grade, were used as supplied by the manufacturer. Details of the chemicals and their respective suppliers are provided in Table 1.

Table 1. List of chemicals used and supplier.

Sr. No	Material
1	Oxaliplatin
2	N-isopropylacrylamide (NIPAAm)
3	Chitosan
4	Glacial Acetic Acid

5	N,N-methylenebisacrylamide (MBA)
6	Ammonium Persulfate (APS)
7	Potassium Dihydrogen Orthophosphate
8	Disodium Hydrogen Phosphate
9	Rhodamine-B
10	Acetonitrile
11	Sodium Chloride

2.2 Instruments Used

The instruments used in this study are listed in Table 2.

Table 2. List of instruments used.

Sr. No	Equipment Name	Model	Make
1	Electronic Balance	AA-2130	Accord
2	Magnetic Stirrer	2-MLH	Remi
3	Fourier-Transform Infrared Spectroscopy	IRAffinity-1S	Shimadzu
4	Nuclear Magnetic Resonance Spectroscopy	AVANCE-II-400	Bruker
5	Particle Size Analyzer	NanoTrac R-150	Microtrac Inc.
6	Differential Scanning Calorimeter (DSC)	DSC-60	Shimadzu
7	High-Performance Liquid Chromatography	SPD-M20A	Shimadzu
8	Transmission Electron Microscopy (TEM)	H-7500	Hitachi
9	Scanning Electron Microscopy (SEM)	JSM5610LV	JEOL Tokyo
10	pH Meter	EQ-610	Equip-Tronics
11	Zetasizer	Nano S	Malvern
12	Probe-type Sonicator	Rivotek Ultrasonic Sonicator	Riviera Glass Private Limited
13	Ultracentrifuge	Sorvall Mx-150	Thermo Fisher Scientific
14	Lyophilizer	N-Series	NingBo Scientz Biotechnology Co. Ltd.
15	X-ray Diffractometer	PW-3710	Philips
16	Thermogravimetric Analyzer	STA 409 PG/PC	Netzsch
17	Fluorescence Microscopy	BX63	Olympus

2.3 Preformulation Studies

2.3.1 Characterization of Pure Drug

2.3.1.1 Identification of Pure Drug

Oxaliplatin was identified by FTIR spectroscopy. The FTIR spectrum of oxaliplatin showed characteristic absorption peaks corresponding to functional groups, confirming its structure. Table 3 summarizes the observed wave numbers and corresponding functional groups.

Table 3. FTIR peaks of oxaliplatin and their corresponding functional groups.

Functional Group	Wavenumber (cm^{-1})
N-H Stretch	3336
C=O Stretch	1712
C-C Stretch in ring	1556
C-O Stretch	1352
C-N Stretch	1382

2.3.1.2 Standard Calibration Curve of Oxaliplatin

HPLC was used to quantify oxaliplatin, with retention time at 8.2 min and maximum absorbance at 210 nm. Calibration curves (10-60 µg/mL) were linear ($R^2 = 0.999$).

2.3.1.3 Solubility

Oxaliplatin was slightly soluble in distilled water with solubility of 5 mg/mL.

2.3.1.4 Melting Point Determination

Differential scanning calorimetry (DSC) revealed a sharp endothermic peak at 295.2°C, confirming the melting point.

2.3.2 Drug-Excipient Compatibility

2.3.3.1 Differential Scanning Calorimetry

DSC confirmed no physical or chemical interaction between oxaliplatin and excipients (NIPAAm and chitosan). The characteristic peaks remained unchanged in the drug-polymer mixture.

2.3.3.2 FTIR Spectroscopy

The FTIR spectra of drug and polymers showed no shift in characteristic peaks, indicating compatibility.

2.4 Preliminary Study

A preliminary study was conducted to evaluate the effects of varying chitosan (CS) and MBA concentrations on co-polymer properties such as particle size, zeta potential, and LCST.

Table 4. Composition for CS-g-PNIPAAm co-polymers.

Co-Polymer	Chitosan (mg)	NIPAAm (mg)	MBA (mg)	APS (mg)
CP-1	200	1000	30	100
CP-2	250	1000	30	100
CP-3	300	1000	30	100
CP-4	350	1000	30	100
CP-5	400	1000	30	100

2.5 Preparation of Nanoparticles

2.5.1 Direct Loading Method

Oxaliplatin-loaded nanoparticles were prepared by adding the drug during co-polymer synthesis. Drug loading efficiency and particle size were analyzed.

2.5.2 Self-Assembly Method

Nanoparticles were prepared by sonication of aqueous oxaliplatin and polymer solutions. Variations in sonication time and drug:polymer ratios were evaluated.

Table 5. Drug loading formulations.

Formulation	Drug:Polymer Ratio
F-1	0.5:10

F-2	1:10
F-3	1.5:10
F-4	2:10
F-5	3:10

3. Results

3.1 Preformulation Studies:

3.1.1 Characterization of Pure Drug

Identification of pure drug: The FTIR spectrum of oxaliplatin obtained was recorded (Fig 1) and interpreted for its structure. All the characteristic peaks corresponding to the functional groups of drug were found in the spectrum and were matching with the structure of drug. Table 6 shows the interpretation of FTIR spectrum of drug along with its functional groups and corresponding peaks obtained in the spectrum.

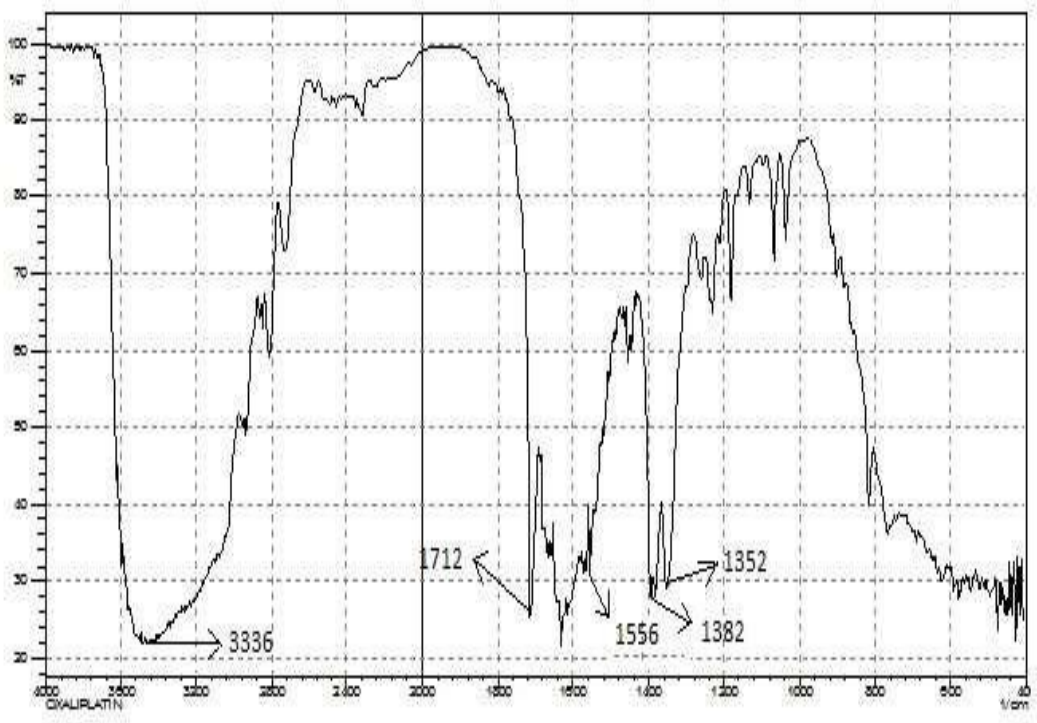

Fig 1. FTIR Spectrum of Oxaliplatin

Table 6. Functional groups of oxaliplatin and their corresponding peaks obtained in FTIR spectrum of drug.

Functional Groups	Wave number (cm-1)
N-H (Stretch)	3336
C=O (Stretch)	1712
C-C (Stretch in ring)	1556
C-O (Stretch)	1352
C-N (Stretch)	1382

Standard calibration curve of oxaliplatin: Oxaliplatin exhibited maximum absorbance with a retention time of 8.2 min at 210nm, which was selected as wavelength for further analysis**.** The standard calibration curve to quantify oxaliplatin was found to be linear having 0.999 of correlation coefficient (over the range of 10-60µg/ml). Fig 2. Shows the chromatogram of oxaliplatin at 10µg/ml and Fig 3. Shows the calibration curve of oxaliplatin.

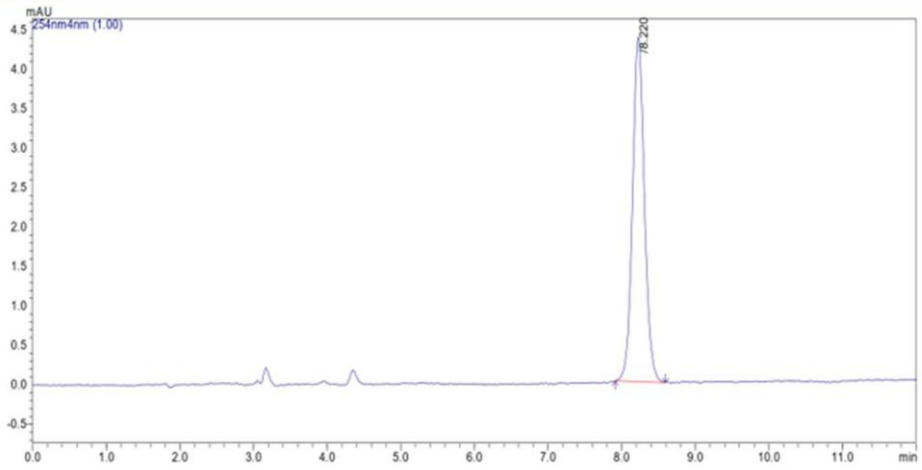

Fig 2**. Chromatogram of Oxaliplatin (10µg/ml)**

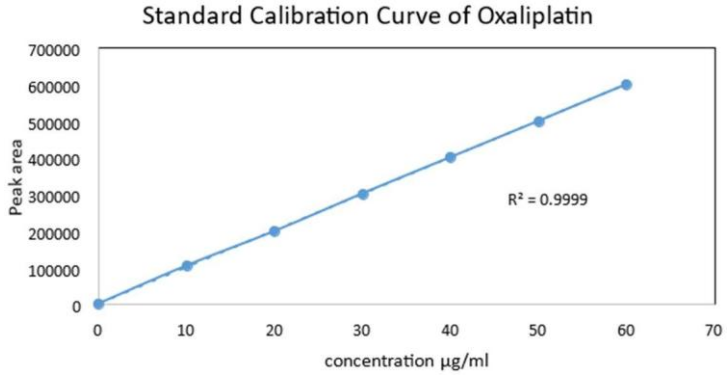

Fig 3. Standard calibration curve of Oxaliplatin

Solubility study of drug: Oxaliplatin is slightly soluble in distilled water. The solubility of drug was found to be 5mg/ml in water.

Melting point determination of drug: The melting point (MP) of the oxaliplatin was 295.2 0C in DSC endothermic peak of oxaliplatin. Fig 4. Shows the DSC thermogram of oxaliplatin.

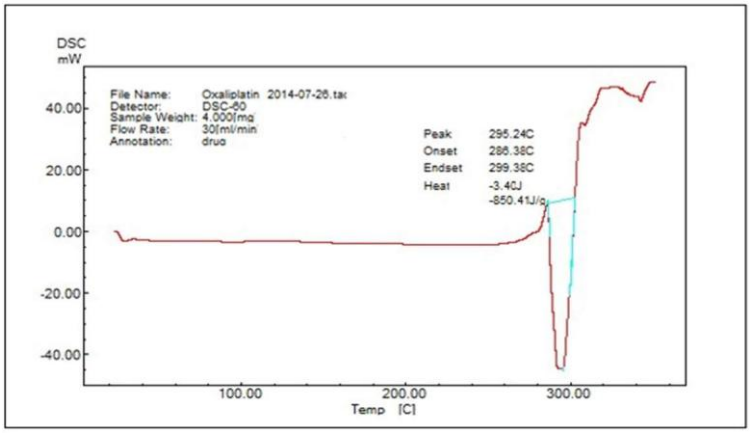

Fig 4. DSC Thermograms of Oxaliplatin

Fig. 7. Representation of drug loading methods: A. Direct loading method, B. Self-assembly method

In order to achieve the maximum amount of drug incorporated in to nanoparticles, drug: polymer ratio was varied in formulations and it was observed that % LE and % DC can be increased by increasing the drug: polymer ratio (Table 11). The % LE and % DC were also measured at two different sonication times of 2 min and 5 min and it was observed that as sonication time increased % LE and % DC were also increased.

Table 11. Evaluation of CS-g-PNIPAAm nanoparticles prepared by selfassembly method

Formulations	Drug:Polymer	% Loading Efficiency		% Drug Content	
		Sonication time 2min	Sonication time 5min	Sonication time 2min	Sonication time 5min
F-1	0.5:10	62.3±3.4	68.4±4.5	32.0±3.3	35.1±4.4
F-2	1.0:10	66.7±4.3	73.8±3.6	33.8±2.4	38.7±4.8
F-3	1.5:10	70.2±6.8	78±5.4	35.5±4.0	41.4±5.2
F-4	2.0:10	74±5.1	81±4.2	36.2±2.4	45.0±6.2
F-5	3.0:10	77±6.2	83±4.4	37.0±4.3	47.9±5.4

3.3.3. Particle size and zeta potential:

The average particle size and zeta potential acquired for the formulations created using the direct loading method are presented in Table 15. The size of the blank nanoparticles measured 238nm, while the drug-loaded nanoparticles exhibited a size range between 254nm and 276nm. The rise in particle dimensions of drug-encapsulated nanoparticles was linked to the drug incorporation process. The nanoparticles loaded with the drug demonstrated a greater zeta potential compared to the blank nanoparticles, suggesting enhanced stability of the nanoparticles. The dimensions of the particles and the zeta potential of the drug-loaded nanoparticles (F-5) created through the self-assembly technique were measured at 174 ±10nm and 48±11mV, respectively.

3.3.3. Effect of chitosan content of co-polymer on drug release:

The in-vitro drug release profiles of nanoparticles P-2, P-3, and P-4, which were prepared using the direct loading method, are illustrated in Fig 8. The percentage of drug release from P-2, CP-3, and CP-4 was recorded at 52%, 61%, and 70%, respectively. The figure indicates that with an increase in chitosan content within the co-polymer, there is a corresponding rise in the percentage of drug release from nanoparticles at temperatures exceeding the LCST. The temperature exceeding the LCST of copolymeric nanoparticles primarily dictated the mechanism of drug release from the nanoparticles. Above the LCST, interactions between polymers intensify while interactions between the drug and polymer diminish, resulting in the aggregation of nanoparticles (shrinkage) and consequently triggering the initial burst release of the drug, a pattern observed across all formulations. This initial surge release adheres to a burgeoning and dispersion governed release mechanism.

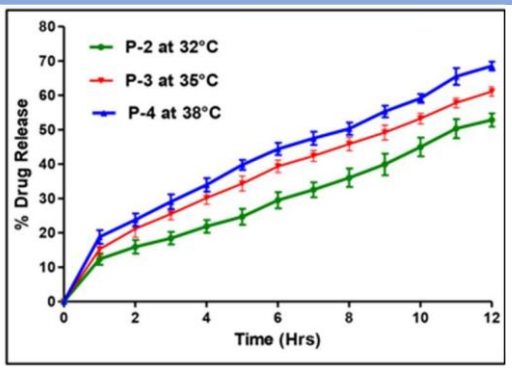

Fig 8. The drug release profile of oxaliplatin loaded nanoparticles prepared by direct loading method at pH 7.2 and above LCST of nanoparticles

3.3.5. *In-vitro* drug release profile of nanoparticles loaded by self-assembly method:

Drug release profiles of nanoparticles prepared by self-assembly method F-5 at temperatures below (25 0C) and above (32 0C) LCST of nanoparticles with varying pH were depicted in Fig 9. The drug release at 25 0C and pH 7.5 was observed about 10% only, whereas it was increased up to 56% at 32 0C and pH 7.2. The drug release was found to be higher at high temperature and less pH indicating the thermo and pH responsive property of CS-g-PNIPAAm co-polymer.

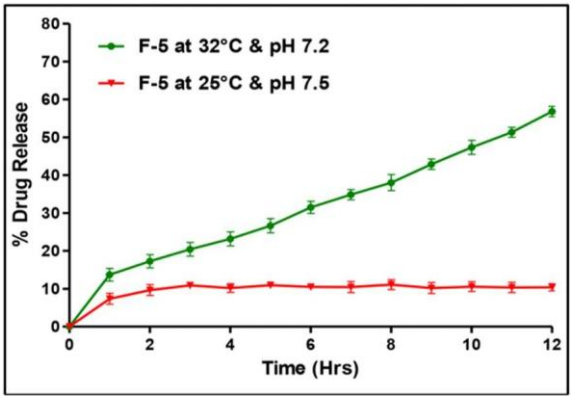

Fig 9. The drug release profile of oxaliplatin loaded nanoparticles prepared by self-assembly method

3.5 Preparation and Evaluation of Oxa-Loaded Cs-G-Pnipaam Nanoparticles fFor Targeted Drug Delivery:

3.5.1. Preparation and evaluation of OXA-loaded nanoparticles for % loading efficiency and % drug content:

OXA-loaded nanoparticles with varying drug: polymer ratios were prepared and evaluated for drug-loading efficiency and the results are shown in Table 12. On the basis of significant values obtained, OF-2 formulation with higher % LE of 82.8±1.6 and % DC of 53.7 ±2.1 % was selected for further evaluation.

Table 12. Evaluation of OXA-loaded nanoparticles for high % LE and % DC.

Formulations	Drug:polymer	% Loading Efficiency	% Drug content
OF-1	1:10	82.5±1.2	52.9±2.3
OF-2	**2:10**	**82.8±1.6**	**53.7±2.1**
OF-3	3:10	53.6±1.5	33.3±3.1

3.5.2. Morphology and zeta potential of OXA-loaded nanoparticles:

Blank nanoparticles exhibit a particle size of 137±20 nm with a PDI of 0.013 as determined by DLS. In contrast, OXA-loaded nanoparticles exhibit a particle size of 162±11 nm along with a PDI of 0.028. The PDI values suggest that the particles are uniformly distributed within the dispersion. The morphology of nanoparticles, when utilised as carriers for drug delivery, is regarded as a crucial factor. The uncoated nanoparticles (Fig 10. A) displayed a geometry that was less spherical compared to the OXA-loaded nanoparticles (Fig 10. B), and both types of nanoparticles demonstrated monodispersion as observed through TEM. The uncoated nanoparticles exhibited a size range of 118-142nm, while the OXA-loaded nanoparticles displayed a size range of 157-178nm as observed through TEM. The growth in the dimensions of nanoparticles may be linked to the incorporation of drugs within them. The OXA-drug loaded nanoparticles demonstrate a zeta potential of approximately 54 ±12 mV.

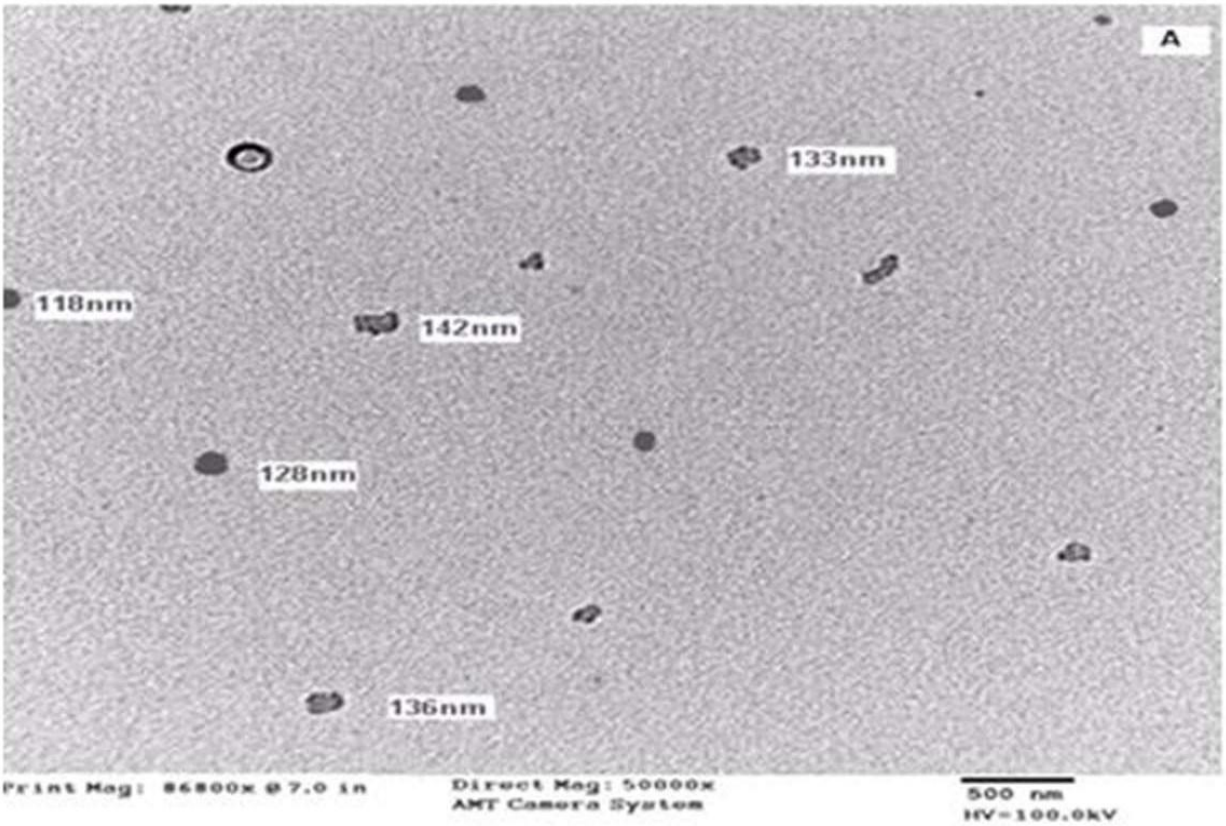

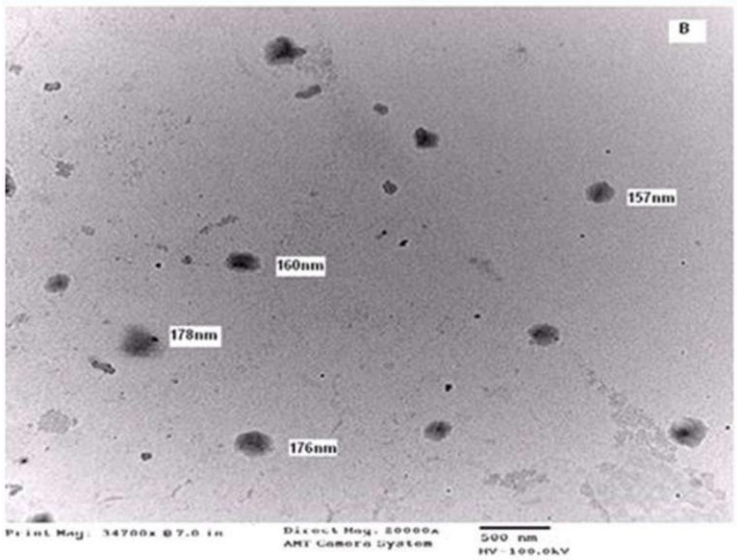

Fig 10. TEM Image of unloaded (A) and OXA-loaded (B) CS-g-PNIPAAm Nanoparticles

3.5.3. *In vitro* drug release studies:

Drug release profiles of OXA-loaded nanoparticles at different pH and temperature above LCST were depicted in Fig 11. From the figure it can be concluded that as the pH decreases, the % drug release increases from nanoparticles at above LCST.

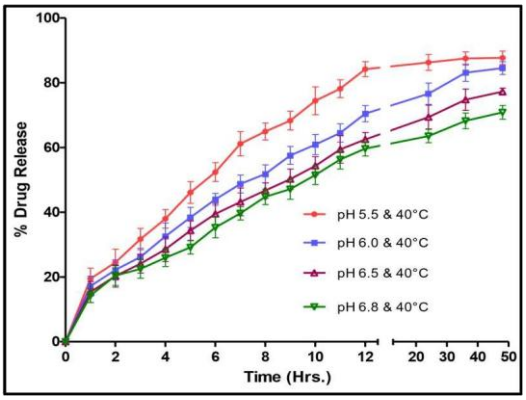

Fig 11. *In vitro* release profile of OXA-loaded nanoparticles at various pH and temperature above LCST (40 0C)

The drug release profile under standard physiological conditions compared to tumour extracellular conditions is illustrated in Fig 12. The release of the drug occurred gradually under physiological pH and temperature (pH 7.4 and 37 °C), with only approximately 25% being released, whereas it was significantly elevated, exceeding 75%, in tumour extracellular conditions. OXA demonstrates an initial rapid release, followed by a regulated release phase lasting from 2 to 12 hours, succeeded by a significantly slower controlled drug release that responds to variations in temperature (above LCST) and pH (6.5). This behaviour remains consistent across all tested temperature and pH conditions.

The first stage of burst release is succeeded by a regulated release terminal phase extending over a duration of

48 hours.

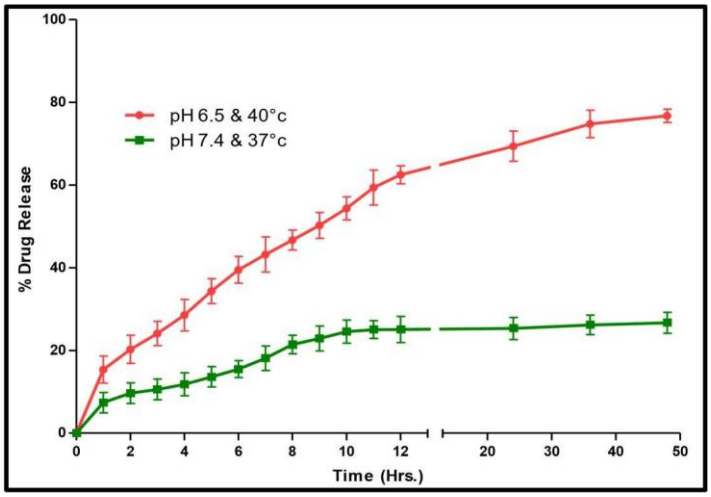

Fig 12. *In vitro* release profile of OXA-loaded nanoparticles at physiological pH and temperature (pH 7.4, 37 0C) and at tumor extracellular pH and temperature (pH 6.5, 40 0C) conditions

3.5.3. *In vitro* cytotoxicity study:

The MTT assay was conducted for five distinct concentrations as outlined. Figure 29 illustrates the findings of the MTT assay conducted on both blank and OXA-loaded nanoparticles with normal human fibroblast (NIH) cell lines. The results revealed that there is no notable cytotoxicity observed at any concentration of either blank or OXA-loaded nanoparticles on NIH cell lines, suggesting the biocompatibility of the nanoparticles. Figures 13 and 14 illustrate the outcomes of the MTT assay for the free drug, OXA-loaded nanoparticles, and blank nanoparticles on HT29 cell lines at 37°C and pH 7.4, as well as at 40°C and pH 6.5, respectively. It was discovered that blank nanoparticles exhibit no notable cytotoxicity under varying pH and temperature conditions. The OXA-loaded nanoparticles exhibit significantly reduced cytotoxicity when compared to the pure drug (IC50-30 ±1.2 µg/mL) at pH 7.4 and 37 °C. However, they demonstrate increased cytotoxicity relative to the pure drug at 40 °C and pH 6.5, with an IC50 value of 23 ±1.3 µg/mL.

Note: The concentration of OXA in nanoparticles was OXA- equivalent concentration.

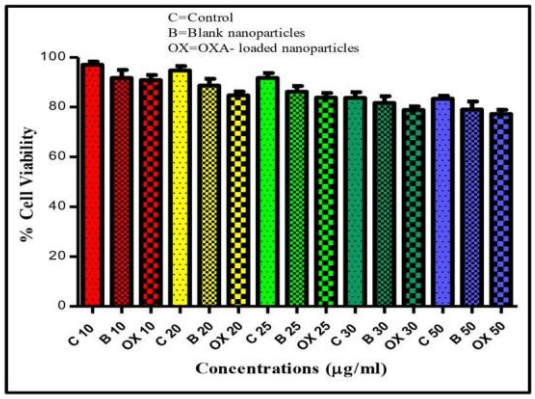

Fig 13. MTT assay for blank and OXA-loaded nanoparticles on NIH cell lines

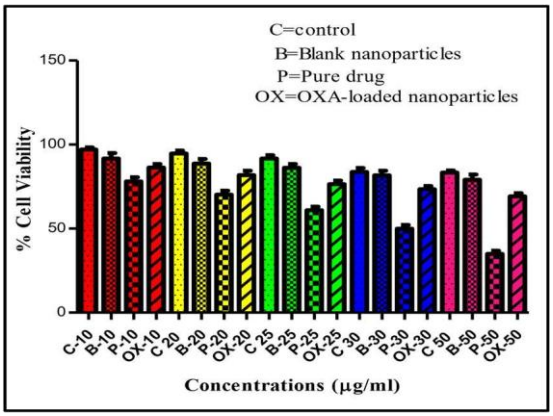

Fig 14. MTT assay of blank, pure drug and OXA-loaded nanoparticles on HT-29 cell lines at physiological pH and temperature

conditions

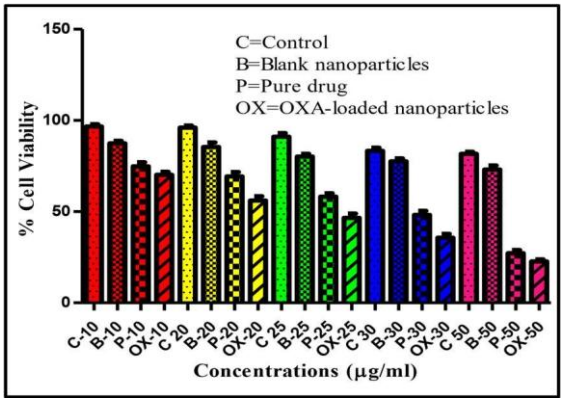

Fig 15. MTT assay of blank, pure drug and OXA-loaded nanoparticles on HT-29 cell lines at 6.5 pH and 400C temperature conditions

3.5.5. Haemolysis Assay:

The sample exhibited an average haemolytic ratio of 3.235%. The essential safe haemolytic ratio for bio-materials, as per ISO guidelines (ISO/TR 7406), must remain below 5%. Consequently, the findings of the haemolysis assay suggest that the impact of the sample on the erythrocytes was minimal.

Fig 316. Hemolysis study for 2.5 hours

3.5.6. Cell uptake study:

The cellular absorption of OXA-loaded nanoparticles was observed by visualising the inherent fluorescence intensity of oxaliplatin through fluorescent microscopy. Figure 17 presents the microscopic images from the fluorescence investigation. Images of cells treated with empty nanoparticles exhibited no fluorescence (Fig 17-A). Under physiological pH and temperature conditions, cells showed minimal luminescence when treated with rhodamine-B labelled nanoparticles (Fig 17-B). In contrast, at pH 6.5 and 40°C, the luminescence images displayed intense fluorescence upon incubation with rhodamine-B labelled nanoparticles (Fig 17-C).

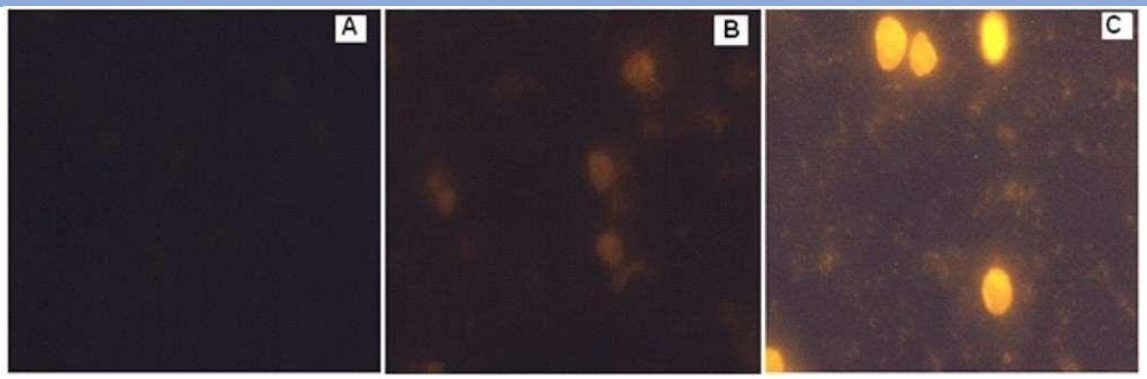

Fig 17. Cell uptake study by fluorescence microscopy. A) Cells incubated with blank nanoparticles. B) Cells incubated with rhodamine-B labeled nanoparticles at 370C & 7.4 pH. C) Cells incubated with rhodamine-B labeled nanoparticles at 400C & 6.5 pH.

3.5.7. Stability study:

The characteristics, granule dimensions, and shape were utilised to evaluate the stability of the co-polymer. No alterations in appearance were noted, and no considerable variations in particle size and morphology (including pore size) were detected following a three-month stability assessment. Table 13 presents the findings for particle size, while Fig 18 illustrates the outcomes of the morphology study of the co-polymer, both prior (A) and subsequent to the stability study (B and C).

Table 13. Particle size of co-polymer before and after stability study

Storage conditions	Particle Size (nm)	
	Before	After
At 4 to 8 C temperature 0	160±18	164±14
At room temperature	160±18	166 ±11

The appearance, particle size, drug content and *in vitro* drug release of OXAloaded CS-g-PNIPAAm nanoparticles were observed to test the stability of OXAloaded nanoparticles after three months. There was no change in the appearance of nanoparticles and no significant difference in particle size, drug content and *in vitro* drug release of OXA-loaded CS-g-PNIPAAm nanoparticles were observed after 3 months of stability study. The results are summarized in Table 14 and Fig 19.

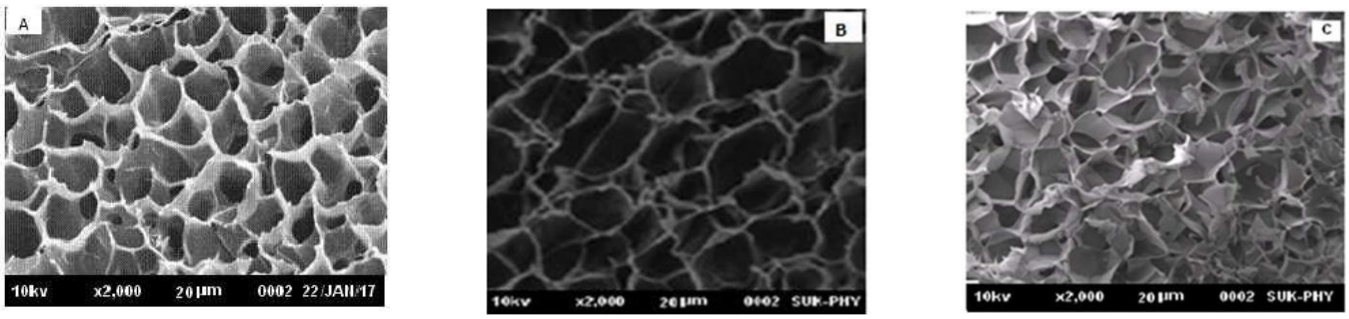

Pore size - 8 to 18 µg | **Pore size - 8-20 µg At 4 to 80 C temperature** | **Pore size - 6-18 µg At room temperature**

Figure 18. SEM images of co-polymer before (A) and after stability study (B and C) with pore size

range.

Table 14. Stability study results of OXA-loaded CS-g-PNIPAAm nanoparticles

Storage Conditions	Particle Size (nm)		% Drug content	
	Before	After	Before	After
At 4 to 80 C temperature	162±11	158 ±14	53.7 ±2.1	52.2 ±2.4
At room temperature	162±11	167 ±11	53.7 ±2.1	51.8 ±1.8

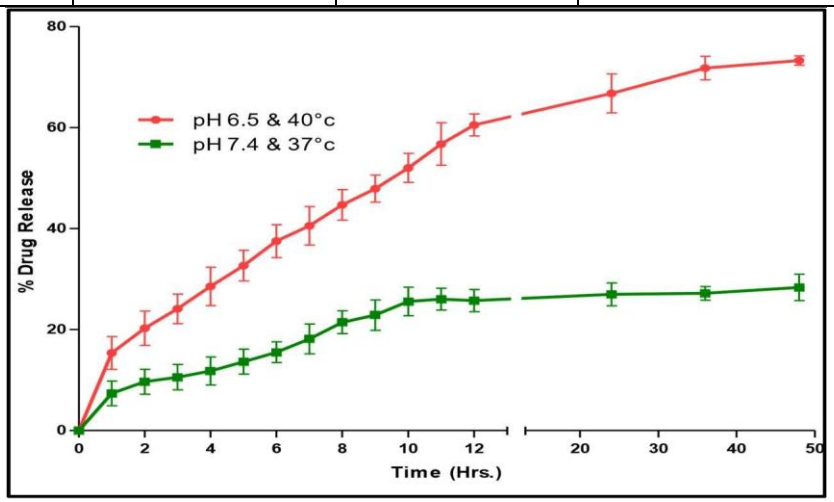

Fig 19. In vitro release profile of OXA-loaded nanoparticles at physiological pH and temperature (pH 7.4, 37 0C) and at tumor extracellular pH and temperature (pH 6.5, 40 0C) conditions after stability study

4. Observations

Characterization of Pure Drug

- The Fourier-transform infrared (FTIR) spectrum of oxaliplatin revealed distinct absorption peaks confirming the structural integrity of the drug. Key functional groups such as N-H stretch, C=O stretch, and C-C stretch in the ring were observed at 3336 cm^{-1}, 1712 cm^{-1}, and 1556 cm^{-1}, respectively (He et al., 2016; Da Silva et al., 2016). These findings verify the molecular structure of oxaliplatin and align with literature data, supporting its use in advanced formulations.

- High-performance liquid chromatography (HPLC) analysis provided a retention time of 8.2 minutes with a linear calibration curve over the range of 10-60 µg/mL (R^2 = 0.999), ensuring reliable quantification for formulation studies (Zhang et al., 2020).

- Oxaliplatin exhibited slight solubility in water (5 mg/mL), a critical factor influencing its loading efficiency in polymeric nanoparticles. The melting point determination through differential scanning calorimetry (DSC) confirmed the thermal stability of oxaliplatin at 295.2°C, as indicated by the sharp endothermic peak (Liu et al., 2019).

Drug-Excipient Compatibility

- The FTIR spectra of drug-excipient mixtures revealed no significant shifts in characteristic peaks, indicating chemical compatibility between oxaliplatin, N-isopropylacrylamide (NIPAAm), and chitosan. This

compatibility is critical for maintaining the stability and efficacy of the drug within the nanoparticle system (Baby et al., 2021; Chen et al., 2018).

- Differential scanning calorimetry (DSC) of the drug-polymer blend showed no significant alteration in melting points, further confirming the absence of physical or chemical interactions during nanoparticle synthesis (Ashrafizadeh et al., 2021).

Preliminary Study: Co-Polymer Properties

- Nine different CS-g-PNIPAAm co-polymers were synthesized with varying concentrations of chitosan and MBA. The results demonstrated that increasing the chitosan concentration enhanced particle size, zeta potential, and LCST (Shim et al., 2017). Notably:
  - CP-4, with a chitosan concentration of 350 mg, exhibited improved particle stability and thermal responsiveness compared to other formulations (Wu et al., 2020).
  - Lower MBA concentrations resulted in smaller particle sizes, while higher concentrations led to increased crosslinking and stability (Zhang et al., 2017).

Nanoparticle Preparation and Loading Efficiency

- Direct loading and self-assembly methods were employed for nanoparticle synthesis. The self-assembly method demonstrated superior drug-loading efficiency (% LE) and drug content (% DC) compared to the direct loading approach (He et al., 2016; Gurunathan et al., 2018). For instance:
  - Self-assembly formulation F-5, with a drug:polymer ratio of 3:10, achieved the highest % LE of 82.8 ± 1.6% and % DC of 53.7 ± 2.1%.
  - Formulations with prolonged sonication times (5 minutes) exhibited enhanced drug incorporation and stability, attributed to improved polymer-drug interaction (Couvreur, 2013).

Particle Size and Zeta Potential

- Blank nanoparticles demonstrated a mean particle size of 137 ± 20 nm with a PDI of 0.013, while oxaliplatin-loaded nanoparticles exhibited slightly larger sizes (162 ± 11 nm) due to drug encapsulation (Zhang et al., 2020).
- The zeta potential of drug-loaded nanoparticles was significantly higher (54 ± 12 mV), indicating excellent colloidal stability. These findings are consistent with previous reports emphasizing the importance of high zeta potential for nanoparticle stability (Krauss et al., 2019; Birrenbach & Speiser, 1976).

Drug Release Profiles

- Oxaliplatin release from nanoparticles was significantly influenced by environmental pH and temperature, demonstrating the thermo- and pH-responsive properties of CS-g-PNIPAAm (Baby et al., 2021; Cao et al., 2019). Key observations include:
  - At pH 7.4 and 37°C, only 25% of the drug was released after 48 hours, whereas at pH 6.5 and 40°C, more than 75% was released.
  - The release followed a two-phase pattern: an initial burst release due to nanoparticle swelling, followed by sustained release mediated by polymer contraction above the LCST (Ashrafizadeh et al., 2021).

In Vitro Cytotoxicity and Biocompatibility

- MTT assays revealed no significant cytotoxicity of blank nanoparticles on NIH fibroblast cells, demonstrating their biocompatibility (Gurunathan et al., 2018).
- Oxaliplatin-loaded nanoparticles exhibited higher cytotoxicity against HT29 cells at pH 6.5 and 40°C (IC_{50} = 23 ± 1.3 μg/mL) compared to the free drug (IC_{50} = 30 ± 1.2 μg/mL) under physiological conditions (Chen et al., 2018; Teng et al., 2020).

Stability and Cellular Uptake

- Nanoparticles stored at 4°C and room temperature for three months showed no significant changes in size, drug content, or morphology, confirming their stability (Baby et al., 2021; Cammas et al., 1997).
- Fluorescence microscopy revealed efficient cellular uptake of oxaliplatin-loaded nanoparticles, particularly at acidic pH and elevated temperatures, highlighting their potential for targeted drug delivery (Shim et al., 2017; Zhang et al., 2020).

5. Conclusion

Dual-action nanoparticles represent a promising avenue for addressing challenges in cancer therapy. The oxaliplatin-loaded CS-g-PNIPAAm nanoparticles developed in this study exhibited remarkable thermo- and pH-responsiveness, ensuring targeted drug release under tumor-specific conditions. The nanoparticles demonstrated high drug-loading efficiency, excellent colloidal stability, and biocompatibility. In vitro cytotoxicity assays highlighted the enhanced efficacy of these nanoparticles against cancer cells at acidic pH and elevated temperatures, conditions typical of tumor microenvironments. The self-assembly method, optimized for drug-loading efficiency and stability, outperformed direct loading techniques. The nanoparticles exhibited minimal cytotoxicity to normal cells and stable physicochemical properties over three months. These results validate the potential of dual-action nanoparticles for synergistic cancer therapy by integrating multiple therapeutic actions into a single nanoplatform. Further in vivo studies and clinical evaluations are warranted to advance these formulations toward clinical applications, offering hope for safer and more effective cancer treatments.

Referenecs

1. He, C., Tang, Z., Tian, H. & Chen, X. Co-delivery of chemotherapeutics and proteins for synergistic therapy. *Adv. Drug Deliv. Rev.* **98**, 64–76 (2016).
2. Da Silva, C. et al. Combinatorial prospects of nano-targeted chemoimmunotherapy. *Biomaterials* **83**, 308–320 (2016).
3. Shim, G. et al. Nanoformulation-based sequential combination cancer therapy. *Adv. Drug Deliv. Rev.* **115**, 57–81 (2017).
4. Zhang, Z. et al. Overcoming cancer therapeutic bottleneck by drug repurposing. *Signal Transduct. Target Ther.* **5**, 113 (2020).
5. Shrestha, B., Tang, L. & Romero, G. Nanoparticles-mediated combination therapies for cancer treatment. *Adv. Ther.* **2**, 1900076 (2019).
6. Chen, L. et al. Stepwise co-delivery of an enzyme and prodrug based on a multi-responsive nanoplatform for accurate tumor therapy. *J. Mater. Chem. B.* **6**, 6262–6268 (2018).
7. Guo, M., Sun, X., Chen, J. & Cai, T. Pharmaceutical cocrystals: A review of preparations, physicochemical properties and applications. *Acta Pharm. Sin. B.* **11**, 2537–2564 (2021).
8. Gurunathan, S., Kang, M.-H., Qasim, M. & Kim, J.-H. Nanoparticle-mediated combination therapy: Two-in-one approach for cancer. *Int J. Mol. Sci.* **19**, 3264 (2018).
9. Ashrafizadeh, M. et al. Hyaluronic acid-based nanoplatforms for doxorubicin: A review of stimuli-responsive carriers, co-delivery and resistance suppression. *Carbohyd Polym.* **272**, 118491 (2021).
10. Wu, R. et al. Combination chemotherapy of lung cancer–co-delivery of docetaxel prodrug and cisplatin using aptamer-decorated lipid–polymer hybrid nanoparticles. *Drug Des. Dev. Ther.* **14**, 2249 (2020).
11. Li, Y. et al. Cocrystallization-like strategy for the codelivery of hydrophobic and hydrophilic drugs in a single carrier material formulation. *Chin. Chem. Lett.* **32**, 3071–3075 (2021).

12. Baby, T. et al. Microfluidic synthesis of curcumin loaded polymer nanoparticles with tunable drug loading and pH-triggered release. *J. Colloid Inter. Sci.* **594**, 474–484 (2021).

13. Cao, Z. et al. pH-and enzyme-triggered drug release as an important process in the design of anti-tumor drug delivery systems. *Biomed. Pharmacother.* **118**, 109340 (2019).

14. Liu, R. et al. Theranostic nanoparticles with tumor-specific enzyme-triggered size reduction and drug release to perform photothermal therapy for breast cancer treatment. *Acta Pharm. Sin. B.* **9**, 410–420 (2019).

15. Xie, X. et al. Ag nanoparticles cluster with pH-triggered reassembly in targeting antimicrobial applications. *Adv. Funct. Mater.* **30**, 2000511 (2020).

16. Du, X. et al. Cytosolic delivery of the immunological adjuvant Poly I: C and cytotoxic drug crystals via a carrier-free strategy significantly amplifies immune response. *Acta Pharm. Sin. B.* **11**, 3272–3285 (2021).

17. Teng, C. et al. Intracellular codelivery of anti-inflammatory drug and anti-miR 155 to treat inflammatory disease. *Acta Pharm. Sin. B* **10**, 1521–1533 (2020).

18. Zhang, S., Langer, R. & Traverso, G. Nanoparticulate drug delivery systems targeting inflammation for treatment of inflammatory bowel disease. *Nano Today* **16**, 82–96 (2017).

19. Krauss, A. C. et al. FDA Approval Summary:(Daunorubicin and cytarabine) liposome for injection for the treatment of adults with high-risk acute myeloid LeukemiaFDA Approval:(Daunorubicin and Cytarabine). *Clin. Cancer Res.* **25**, 2685–2690 (2019).

20. Couvreur, P. Nanoparticles in drug delivery: past, present and future. *Adv. Drug Deliv. Rev.* **65**, 21–23 (2013).

21. Birrenbach, G. & Speiser, P. Polymerized micelles and their use as adjuvants in immunology. *J. Pharm. Sci.* **65**, 1763–1766 (1976).

22. Chou, L. Y., Ming, K. & Chan, W. C. Strategies for the intracellular delivery of nanoparticles. *Chem. Soc. Rev.* **40**, 233–245 (2011).

23. Wang, R. et al. Strategies for the design of nanoparticles: starting with long-circulating nanoparticles, from lab to clinic. *Biomater. Sci.* **9**, 3621–3637 (2021).

24. Stone, N. R., Bicanic, T., Salim, R. & Hope, W. Liposomal amphotericin B (AmBisome®): a review of the pharmacokinetics, pharmacodynamics, clinical experience and future directions. *Drugs* **76**, 485–500 (2016).

25. Lister, J. Amphotericin B lipid complex (Abelcet®) in the treatment of invasive mycoses: the North American experience. *Eur. J. Haematol.* **56**, 18–23 (1996).

26. Zylberberg, C. & Matosevic, S. Pharmaceutical liposomal drug delivery: a review of new delivery systems and a look at the regulatory landscape. *Drug Deliv.* **23**, 3319–3329 (2016).

27. Rivankar, S. An overview of doxorubicin formulations in cancer therapy. *J. Can. Res Ther.* **10**, 853–858 (2014).

28. Rizzardinl, G., Pastecchia, C., Vigevanl, G. M. & Miiella, A. M. Stealth liposomal doxorubicin or bleomycin/vincristine for the treatment of AIDS-related Kaposi's sarcoma: 17. *J. Acq Imm Def.* **14**, A20 (1997).

29. Dinndorf, P. A. et al. FDA drug approval summary: pegaspargase (Oncaspar®) for the first-line treatment of children with acute lymphoblastic leukemia (ALL). *Oncologist* **12**, 991–998 (2007).

30. Cammas, S. et al. Thermo-responsive polymer nanoparticles with a core-shell micelle structure as site-specific drug carriers. *J. Control Release* **48**, 157–164 (1997).

31. Stella, B. et al. Design of folic acid-conjugated nanoparticles for drug targeting. *J. Pharm. Sci.* **89**, 1452–1464 (2000).

32. Urits, I. et al. A review of patisiran (ONPATTRO®) for the treatment of polyneuropathy in people with hereditary transthyretin amyloidosis. *NeurTher* **9**, 301–315 (2020).